Improving textural properties of magnesium-based metal-organic framework for gas adsorption by carbon doping

Khaliesah Kamal, Denys Grekov, Azmi Mohd Shariff, Mohamad Azmi Bustam, Pascaline Pré

Improving textural properties of magnesium-based metal-organic framework for gas adsorption by carbon doping

Khaliesah Kamal[1,2], Denys I. Grekov[1], Azmi Mohd Shariff[2], Mohamad Azmi Bustam[3,*], Pascaline Pré[1,*]

[1]GEPEA Laboratory, Department of Environment and Energy Systems (DSEE), IMT Atlantique, UMR-CNRS 6144, 44300 Nantes, France.

[2]CO_2 Research Centre (CO2RES), Department of Chemical Engineering, Universiti Teknologi PETRONAS, 32610 Perak, Malaysia.

[3]Centre of Research in Ionic Liquids (CORIL), Department of Chemical Engineering, Universiti Teknologi PETRONAS, 32610 Perak, Malaysia.

*Corresponding Authors: Mohamad Azmi Bustam (azmibustam@utp.edu.my), Pascaline Pré (pascaline.pre@imt-atlantique.fr)

Abstract:

A magnesium-based metal-organic framework (MOF), Mg-MOF-74, has been denoted as a landmark for CO_2 capture due to its highly porous structure and strong metal adsorptive sites. However, the gas uptake would be improved if particle texture could favor diffusion into the micropores and accessibility to the adsorption sites. For that reason, multi-wall carbon nanotubes (CNT) or monolayer graphene oxide (GO) was introduced into the MOF material at 0.3 wt% via in-situ synthesis method as an attempt to improve gas adsorption capacities. Mg-MOF-74, Mg-MOF-74@CNT and Mg-MOF-74@GO were synthesized under solvothermal reaction and characterized by PXRD, FTIR, FESEM, TGA and N_2@77K and CO_2@298K adsorption/desorption analysis. The morphology of the Mg-MOF-74 composites showed that the particles composed of agglomerated crystallites of which the crystal structure was well-preserved with the adjunction of carbon doping agents. The BET specific surface area and the micropore volume of the Mg-MOF-74 pristine material respectively attained 1370 m^2/g and 0,4 cm^3/g whilst these values were increased up to 1660-1720 m^2/g and ~0.49 cm^3/g for carbon composites. These variations were attributed to better activation of carbon-MOF composites thanks to more regular arrangement of the crystallites composing the agglomerates, facilitating the evaporation of the organic solvent during the thermal treatment applied in the last stage of the synthesis. The introduction of a small fraction of CNT and GO in the reactant mixture also improves the crystallization process, leading to average larger particle sizes. Consequently, the uptake of CO_2 at 1 bar and 25 °C was shown to be improved by 18 mol% and 23 mol% for Mg-MOF-74@CNT and Mg-MOF-74@GO, respectively, compared with the pristine Mg-MOF-74. This current work demonstrates that by doping Mg-MOF-74 synthesis with carbonaceous agents, although at very low concentration

levels, both morphological and textural properties are modified leading to larger gas adsorption capacities.

Keywords:

Metal-organic framework, MOF-74, MOF-carbon composite, Graphene oxide, Carbon nanotubes, Gas adsorption

Introduction:

Owing to the ability to provide large microporous volumes and high specific surface areas, metal-organic frameworks (MOFs) have been an object of intense research in numerous contexts such as nanocatalysis [1], drug delivery [2], removal of hazardous substances [3], removal of key odorants [4] and development of electrode materials for electrochemical detectors and energy storage devices [5]. Since MOF materials may develop specific surface area as high as 6240 m^2/g [6], one of their most promising applications is the processes of gas storage and separation relying on adsorption [7]. Moreover, by reason of well-defined structure of micropore walls, MOFs are also recognized for the possibility of fine and controlled tuning of gas adsorption properties by performing ligand design, metallic center substitution or functionality adjustment [8]. This allows to rich gas adsorption capacity and separation selectivity that cannot be achieved by other porous materials [9].

To date, MOF-74 family and particularly Mg-MOF-74 material figure among the most promising adsorbents for CO_2 separation from CH_4/CO_2 and $CH_4/CO_2/N_2$ gas streams in the context natural gas and biogas purification [10-12]. Characterized by BET specific surface area close to 1200 m^2/g [13] and one-dimensional pores of approximately 10 Å [14], this material features exceptional density and accessibility of open metal sites which are the preferential adsorptive centers for gas molecules [15]. The ratio of Henry constants of CO_2 and CH_4 adsorption exhibited by Mg-MOF-74 is reported as high as 330 allowing one of the best efficiency of CO_2/CH_4 separation by MOF materials [16]. This excellent selectivity towards CO_2 originates from strong intermolecular interactions of this gas with the exposed metallic centers leading to the stabilization of their coordination sphere and thus high ordering of adsorbed CO_2 molecules within unit cell as revealed by different in-situ characterization

techniques [11, 14, 17].

Further improvement of gas adsorption performances of MOF materials can be achieved by optimizing the texture and morphology of the solid creating additional microporosity and interstitial porosity [18-20]. This facilitates gas transport to adsorption sites and increases total accessible pore volumes and specific surface areas. A number of structural and functional modifications from virgin MOFs have been proposed as strategies to attain this purpose. Recently, researches on incorporation of MOFs with carbon-based compounds from which MOF-carbon composites are produced are continuously being conducted. By virtue of the formation of secondary micro- and mesoporosity, the synthesized composites have been reported able to increase gas adsorption capacity and separation efficiency in comparison to their parent materials [12, 21-33].

The preparation of MOF composites, specifically for gas adsorption application, must involve the formation of MOF units in continuous phase applying either three common approaches: (i) post-synthesis, and, in-situ synthesis type (ii) ship-in-a-bottle or (iii) bottle-around-ship methods [18]. Post-synthetic modification can be performed via procedure of simple loading (impregnation), insolubilization (coprecipitation), encapsulation, chemical conversion, infiltration or functionalization as recently reported by Ullah et al. (2020) in preparing MOF-200-carbon composite [34]. In-situ synthesis ship-in-a-bottle method refers to the formation of a composite from “preformed MOFs” and “doping agent precursors” during the reaction in the synthesis procedure. Described as encapsulation of doping material by MOF units, the doping precursors penetrate into MOF pores by means of diffusion in liquid media. The composite is formed by stabilizing the formation of doping material inside MOF pores using chemical or thermal method. Due to the increase in size, the final particle of doping material

remains stable inside MOF pores. This method is early well-known for zeolite composites [35] and recently adopted for MOF composites [36].

Different from the previous approach, in-situ synthesis bottle-around-ship method is carried out by direct mixing "MOF precursors" with "doping agent particles" before the reaction in the synthesis procedure. The MOF units are built from the precursors around the doping material leading to the trapped and immobilized large particles of doping agent within MOF units after complete formation. Adopted for this work, this method is widely published for the preparation of MOF-carbon composites for the application of gas adsorption [12, 21-33]. However, for in-situ synthesis, an appropriate amount of carbon doping material is required to prevent excessive interference with the coordination reactions of MOFs that may ruin the structure of MOF-carbon composites and adversely affect the performance of the material [19]. Therefore, an optimization study of substitution composition of the doping material is primordial.

Inspired by the above thoughts, Mg-MOF-74-carbon composites were synthesized and characterized in this work with the aim of improving textural and morphological properties of Mg-MOF-74 for gas adsorption. Two carbonaceous materials, multiwalled carbon nanotubes (CNT) and monolayer graphene oxide (GO) were used as doping agents.

Materials and Methods:

1. Materials:

All reagents were commercially available and consumed as received. Magnesium nitrate hexahydrate [$Mg(NO_3)_2 \cdot 6H_2O$ ≥99%, Merck], 2,5-dihyroxyterephtalic acid (dobdc, 98%, Aldrich), n,n-dimethylformamide (DMF, 99.8%, Merck), ethanol absolute (99.8%, BDH),

methanol (99.9%, Merck), graphene oxide (GO monolayer content >95%, oxygen content ≥36%, 4 mg/mL, dispersion in H_2O, Sigma-Aldrich) and carbon nanotubes (multiwalled CNT >7.5% basis, 7-15 nm diameter, 0.5-10 μm length, >99% purity, Sigma-Aldrich) were all purchased from Portray (M) Sdn Bhd.

2. Synthesis:

2.1. Synthesis of pristine Mg-MOF-74:

The protocol employed was adapted from the synthesis method described by Bao et al. (2011) [13]. It includes additional separation steps by centrifugation during the washing process and applies an activation temperature reduced from 250 °C to 150 °C [37]. In details, 712 mg of soluble metal salt $Mg(NO_3)_2 \cdot 6H_2O$ and 167 mg of dobdc linker were completely dissolved in a 15:1:1 (v/v/v) mixture of DMF, ethanol and water using ultrasonication. The homogeneous solution was then transferred into a 125-ml Teflon lined stainless-steel autoclave reactor and left in the oven at 125 °C for 26 h. Then, the product was washed 3 times with methanol using centrifugation and then it was immersed in methanol for 3 days. The product was separated from the washing solvent using centrifugation and dried in a vacuum oven at 80 °C. The remaining solvent was evacuated under a dynamic vacuum at 150 °C for 15 h. The produced Mg-MOF-74 was the pristine material in this work.

2.2. Synthesis of Mg-MOF-74@GO and Mg-MOF-74@CNT composites:

The carbon doping agent was added before the ultrasonication in the above procedure by direct mixing as reported elsewhere [12]. CNT or GO was measured in mass-basis to obtain 0.3% of the weight of the pristine Mg-MOF-74. The substitution percentage was optimized accounting for maximization of CO_2 adsorption uptake à 25 °C, 1 atm. The composites were designated as Mg-MOF-74@CNT and Mg-MOF-74@GO, respectively.

After synthesis, pristine Mg-MOF-74 and its carbon composites were stored in tight glass flasks inside sealed bags over dehydrated silica gel.

3. Structural and textural characterization:

3.1. Powder X-Ray Diffraction analysis (PXRD):

The crystalline structure of the samples was confirmed by using powder X-ray diffraction. XRD patterns were recorded by using Bruker AXS - D8 Advance Diffractometer with Cu Kα radiation (λ=1.5406 Å), step size of 0.02° in 2θ ranged from 5° to 45° and scan rate of 1°/min.

3.2. Fourier-Transform Infrared Spectroscopy analysis (FTIR):

FTIR spectra were recorded by using Nicolet 400D Shimadzu Spectrometer in 4000-500 cm^{-1} region. The spectra with the resolution of 4 cm^{-1} were acquired in Attenuated Total Reflection (ATR) mode allowing direct measurement of powder samples under ambient conditions within 32 scans. For every measurement, the background scanning was performed to reduce the contribution of air and impurities such as carbon dioxide.

3.3. Field Emission Scanning Electron Microscopy analysis (FESEM):

Zeiss SUPRA 55VP instrument was used to study the morphology of the samples. The micrographs were visualized from 1k to 100k magnification using secondary electrons detector. The sample powder was deposited onto a conductive carbon double-sided adhesive tape on a specimen stub. The loose material was removed. The sample coating was effectuated with a platinum sputter coater for 60 s. The sample was placed in a vacuum chamber where the applied vacuum reached an optimum value of $p=2\cdot10^{-5}$ bar before the imaging was run. Energy dispersive X-ray spectroscopy (EDXS) analysis was carried out to access the concentration of different elements on sample surfaces.

3.4. Thermogravimetric analysis (TGA):

TGA measurements were performed on a Setaram LabSys evo TGA-DTA apparatus with temperature ramp from 50 °C to 600 °C at 2 °C/min under flow of helium gas to homogenize heat transfer, protect the balance and avoid sample oxidation. In order to account for mass variation induced by factors other than sample weight loss, the TGA thermogram measured for an empty crucible is systematically subtracted from that of the sample.

3.5. Nitrogen physisorption analysis:

Textural properties of the materials were characterized by using N_2 adsorption/desorption isotherm at 77 K. The isotherms were obtained using 3Flex manometric adsorption analyzer from Micromeritics. The instrument is equipped with pressure transducers allowing measurements in the domain of relative pressure (p/p°) ranging between 10^{-7} and 1 with 0.15% precision of absolute pressure reading. The acquisition was performed in a fixed-dose mode until $p/p^\circ=0.03$ and then incrementing relative pressure. The periodicity of equilibration time measurement in the domain of micropore filling was set to 90 s in order to achieve a complete equilibrium. Before the measurement, the sample was outgassed under dynamic vacuum using Smart VacPrep from Micromeritics at 150 °C for at least 72 h until residual pressure stabilization was achieved. The volumes of cell non-occupied by sample were determined at ambient temperature and at 77 K by helium expansion. Apparent specific surface area was determined using BET method (N_2 cross section=0.162 nm^2) in the domain of $0.005 \leq p/p^\circ \leq 0.05$ in the way to obtain a positive BET constant.

4. Measurement of CO_2 adsorption isotherm:

CO_2 adsorption isotherm of the synthesized materials were measured at 1 bar and 25 °C using 3Flex manometric adsorption analyzer from Micromeritics. Prior to the measurement, the sample was outgassed under the same conditions as in the above procedure when measuring

N_2 adsorption isotherms. The adsorption temperature was controlled by water bath in a Dewar vessel. About 50 mg of sample was placed in a sample cell. Equilibration times were set to 600 s in order to achieve equilibrium.

Results and Discussions:

The synthesized Mg-MOF-74 appeared as yellowish fine powder while Mg-MOF-74@CNT and Mg-MOF-74@GO featured slightly darker tone. Figure 1 shows XRD patterns of all synthesized materials. The pristine Mg-MOF-74 and both composites exhibit sharp characteristic peaks at 6.9°, 11.9°, 13.7°, 15.3°, 16.8°, 18.1°, 19.4°, 20.5°, 21.7°, 23.8°, 24.7°, 25.7°, 26.6°, 27.5°, 28.4°, 29.2°, 30.0°, 30.8°, 31.6◦, 33.8° and 34.5° being in a perfect agreement with those calculated from reference structure available in crystallographic database (Cambridge Crystallographic Data Centre (CCDC), FIJDOS 265095) [38]. Well-defined sharp peaks of XRD pattern of all three samples confirm that Mg-MOF-74 and its composites have good crystallinity. However, qualitative comparison of experimental data for the Mg-MOF-74 composites with that of the pristine material reveals a light narrowing and intensity diminishing of principal peaks at 6.9° and 11.9° suggesting that the doping implies some structural defects. The presence of CNT and GO featuring characteristic XRD signals at 11.9° and 26.1°, respectively, could not be detected in the Mg-MOF-74 composites by this analysis. In order to get access to lattice parameters, average crystal size and micro strain, refinement of XRD profile and Williamson-Hall plot [39] of the synthesized materials were performed as summarized in Table 1 together with their fitting goodness parameter. The profile fitting requires the best fit simulation affording nearly-perfect difference plot as shown in Figure 1. The results reveal that all synthesized materials exhibit values of lattice parameters close to those calculated from reference molecular structure from the database. It

means that the original lattice structure is well-preserved, indicating that the formation of Mg–dobdc was not ruptured by the carbon doping agents. Considering average crystal sizes, the Mg-MOF-74 composites appear with larger average crystallites than the pristine material suggesting that the carbonaceous doping agent does influence the crystal growth process. Although both Mg-MOF-74 composites present slightly higher micro strain in comparison to the pristine material, the deviations observed are not really significant to definitely conclude. In view of numerous challenges associated with atomic position refinement that might be related to the existence of defects in large-volume lattice cells or the occurrence of preferential orientation of crystallites, we did not perform a thorough Rietveld refinement of XRD profile [40, 41] of the synthesized materials.

Table 1. Crystallographic data of the synthesized materials.

Sample	**Mg-MOF-74**	**Mg-MOF-74@CNT**	**Mg-MOF-74@GO**	**Calculated from Mg-MOF-74 molecular structure [38]**
Crystal system	Trigonal (hexagonal axes)			
Angles	α=β=90°, γ=120°			
Space group	R-3			
Lattice parameters				
***a=b* (Å)**	26.009	26.002	25.986	26.026
***c* (Å)**	6.777	6.782	6.777	6.759
Unit cell volume (Å^3)	3970	3971	3963	3965
Average crystal size (nm)	66.6	72.5	81.7	One-unit cell:
Crystal micro strain (%)	0.022	0.041	0.042	

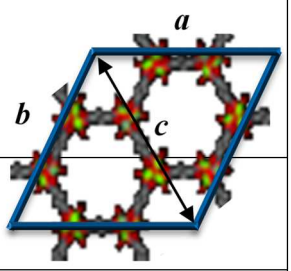

Goodness of fitting	1.95	1.99	1.96	

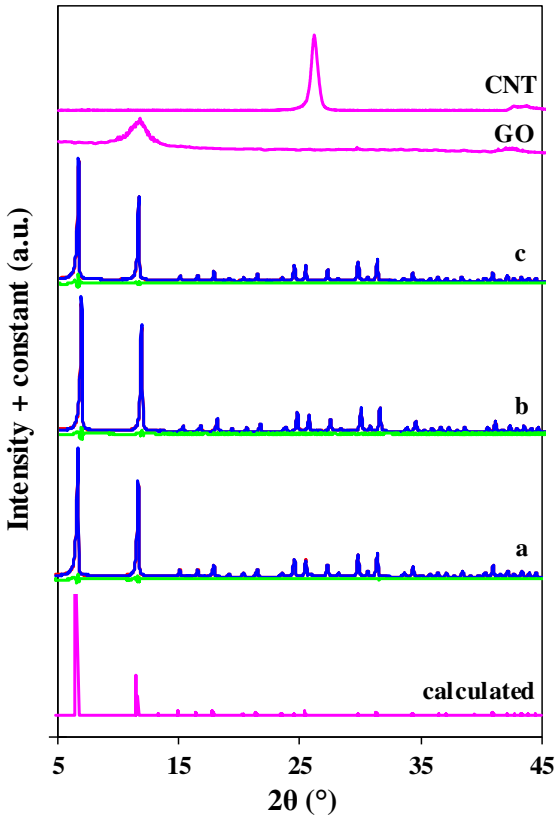

Figure 1. XRD profiles of (a) Mg-MOF-74, (b) Mg-MOF-74@CNT and (c) Mg-MOF-74@GO. Blue, red and green lines represent experimental data, fitting of profile refinement and difference plot, respectively.

In order to assess the effect of ageing on the produced MOF sample, XRD patterns were compared for materials as synthetized and after a 18-month period of storage during which samples were left in sealed bags under anhydrous conditions over a drying agent. Results are given in Figure 1S in Supporting Information. According to DeCoste et al. [42], the structural degradation of Mg MOF-74 crystals caused by humidity can be evidenced by comparing the

ratios of the XRD 6.8° and 11.9° peaks before and after sample exposure to air. This ratio was observed to be considerably reduced after sample exposure to air at 40°C and 40% of relative humidity. According to the same authors, the exposure of Mg MOF-74 for 1 day under air at 40% of relative humidity also results in a dramatic decrease of the specific surface area, falling down to a few m^2/g. In the present study, no such dramatic changes in the peak ratios were reported from the XRD patterns determined for samples as synthesized and after 18 months of ageing under inert conditions (Figure S1-1), neither any significant changes in the measured specific surface areas. The synthesized materials were additionally characterized by FTIR analysis. Figure 2 shows IR spectra of the pristine Mg-MOF-74, both Mg-MOF-74 composites and the linker used in the synthesis. The absence of DMF strong peaks in 3000-2700 cm^{-1} region in MOF spectra confirm that all MOF samples were well-washed from the trace of mother liquor of the reaction. The carboxylate-based linker exhibits a broader O–H stretching band in 3700-2340 cm^{-1} region and stronger C–H alkane stretching vibrations between 3200 and 2500 cm^{-1}. As specified by FitzGerald *et al.*, [43] the growing of the 3700-3200 cm^{-1} band can be attributed to trapped water after a few-minute exposure of MOF materials to ambient air. On the other hand, Tan *et al.* [44], did also the same observation but demonstrated a fully reversible process, after material heating at 150 °C. Both O–H and C–H stretching bands progressively fade during the formation of MOFs. A marginal peak at 1760 cm^{-1} situated in carbonyl region (1840-1740 cm^{-1}) indicates the presence of anhydrides (–CO–O–CO–) before the reaction. A significant peak in the linker at 1500 cm^{-1} is referred to aromatic stretching band of the linker and almost disappears in all MOF spectra. All peaks appeared in 1370-1000 cm^{-1} region signify in-plane C–H bending whereas those in the lower wavenumber region (1000-500 cm^{-1}) indicate out-of-plane C–H bending [45]. It is also

observed that symmetric stretching vibrations of carboxylate groups in all samples are shifted to 1590 cm^{-1} from a lower wavenumber in the linker, 1650 cm^{-1}. Meanwhile, asymmetric stretching vibrations of carboxylate groups in the linker and all samples are observed almost at the same wavelength (1430 cm^{-1}). These carboxylate peaks remain visible in all MOF spectra but with a slight shifting and a significantly reduced intensity, and also, are more pronounced in the pristine Mg-MOF-74 than those of the composites. A small component merging as a shoulder of a symmetric peak at 1590 cm^{-1}, which is the only characteristic peak distinguishing the linker from MOF samples, is observed in Mg-MOF-74 spectrum, indicating the presence of remaining linkers inside micropores, which can be related to the degree of MOF activation. In order to confirm the coordination of carboxylate groups with Mg metal sites at local scale, the separation values between the symmetric and asymmetric peaks were calculated, $\Delta=\lambda_{SYM}(COO^-)-\lambda_{ASSYM}(COO^-)$ [46]. For $\Delta>200$ cm^{-1} and $\Delta<110$ cm^{-1}, monodentate and bidentate ligands are respectively expected, while Δ in the order of 138-200 cm^{-1} represents bridging ligands. The calculated value of Δ(dobdc) is 220 whereas Δ(Mg-MOF-74, Mg-MOF- 74@CNT, Mg-MOF-74@GO) is 160. It is concluded that the carboxylate groups in the linker existed in form of monodentate ligands while in MOFs, the carboxylate groups were deduced binding with Mg cations to form bridging ligands of the framework. Therefore, the formation of the pristine Mg-MOF-74 and the composites were confirmed having similar chemical structure of the ligands which differed from that of the linker before the reaction.

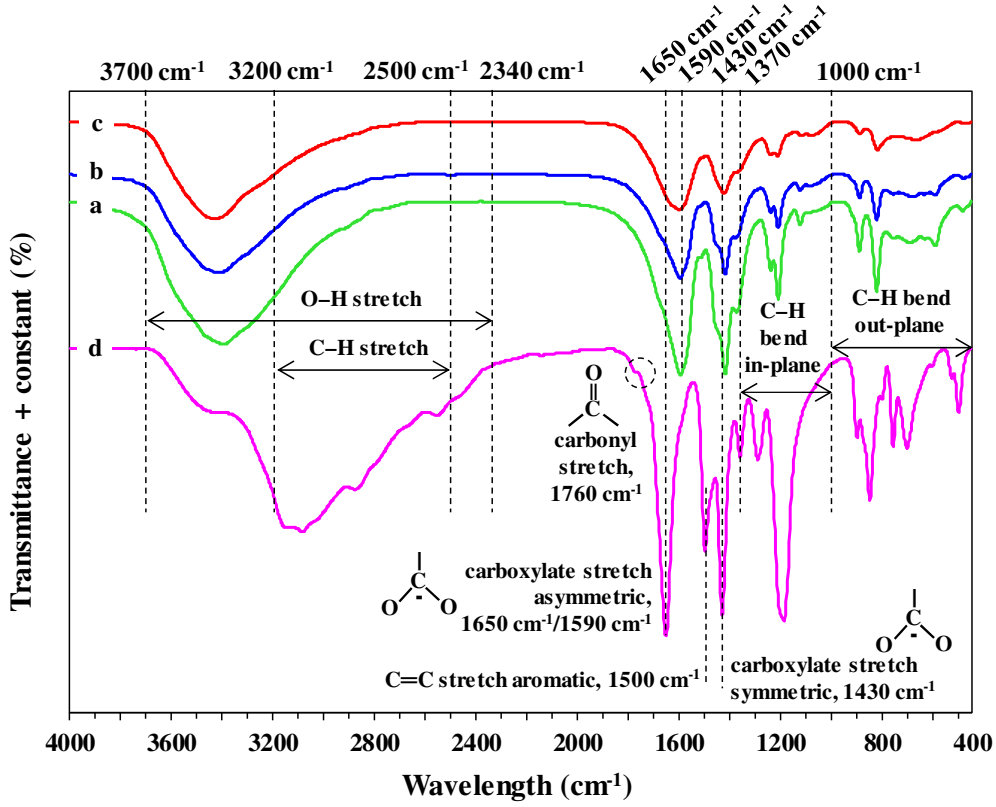

Figure 2. FTIR spectra of (a) Mg-MOF-74, (b) Mg-MOF-74@CNT, (c) Mg-MOF-74@GO and (d) 2,5- dihydroxyterephthalic acid linker.

The morphology of the synthesized materials was examined using FESEM observations as shown in Figure 3. All materials exhibit irregular sizes of hexagonal cylindrical crystallite-like particles which are supposedly referred to the original shape of Mg-MOF-74 (Figure 3i-3iii). The estimation over 30 particles in 83x114 µm image showed that the samples display very wide population of particle sizes of 10-40 µm. However, particle size distribution appears notably different from a material to another. Average particle sizes of single specimen of Mg-MOF-74 (Figure 3i), Mg-MOF-74@CNT (Figure 3ii) and Mg-MOF-74@GO (Figure 3iii) presented in Table 2 show that particles are larger with the addition of CNT and much larger with GO. Interestingly, cross-section of the pristine Mg-MOF-74 particle (Figure 3vii)

exhibits a complex pattern resembling circular staking of plate-like domains with the characteristic thickness on the order of 50-100 nm, corresponding to crystallite size determined from XRD patterns. The interdomain voids feature the size of mesopores which are in the order of tens nm (Figure 3viii). In both Mg-MOF-74 composites, it is noticed that the secondary nucleation of MOF units prevails over the primary growth resulting in pronounced agglomeration of individual particles (Figure 3iv-3vi). In Mg-MOF-74@CNT, some specimens are found randomly agglomerated due to CNT cross-binding through in-and-out of the framework interlocked with the bridging ligands (Figure 3v). The substitution of CNT occurs along with the formation of Mg–dobdc units which made them homogenous and forms agglomerated polycrystalline structure of MOF/CNT (Figure 3ix). The average diameter of the embedded CNT was measured close to 17 nm being in accordance with manufacturer's specification (Figure 3x). In Mg-MOF-74@GO, some specimens tend to form a choral-like agglomeration of crystallites (Figure 3vi) in which GO layers stack in between the planar cage structure of hexagonal MOF crystallites. The attachment of GO layers at crystallite edges causes their architecture became less sharp (Figure 3xi-3xii). Two hypotheses of the synergetic effects between Mg-MOF-74 and GO can be deduced: the growth of some crystals take place on the layers of GO, and, oxygen-functional groups in GO interact with Mg-sites, both of which gave raise to polycrystalline formation MOF/GO. In earlier studies, the interaction of O atoms of GO with Cu-sites of octahedral HKUST-1 was mentioned by Zhao et al. (2014) [22] and Petit et al. (2011) [47] when developed HKUST-1/GO composites. EDXS analysis on material surface reveals slight variances in elementary composition between the different samples. Passing from the pristine Mg-MOF-74 to the composites, a slight increase in Mg atomic content is observed. It can be supposed as the

result of crystallite external surfaces functionalization with carbon doping agents which explains the modification of their morphology. The atomic concentration of O increases by 6-8% in the composites in comparison to the pristine Mg-MOF-74 while C atomic content diminishes by 7-8%. The accuracy of quantitative EDXS analysis is on the order of ±5%, and especially it requires specific sample preparation for the case of "light" elements, so this observation cannot be definitely interpreted. However, higher C content in the pristine Mg-MOF-74 may be due to the presence of residual amount of free ligands enclosed in the micropores which agreed with FTIR results (denoted by a small peak component at 1590 cm^{-1} in the pristine material).

Table 2. Average particle sizes of single specimen and atomic percentage of elements of the synthesized materials.

Sample	**Average particle size of single specimen (μm)**	**Mg (at%)**	**O (at%)**	**C (at%)**
Mg-MOF-74	10	8.32	38.73	52.95
Mg-MOF-74@CNT	23	8.77	46.39	44.84
Mg-MOF-74@GO	37	9.74	44.59	45.66

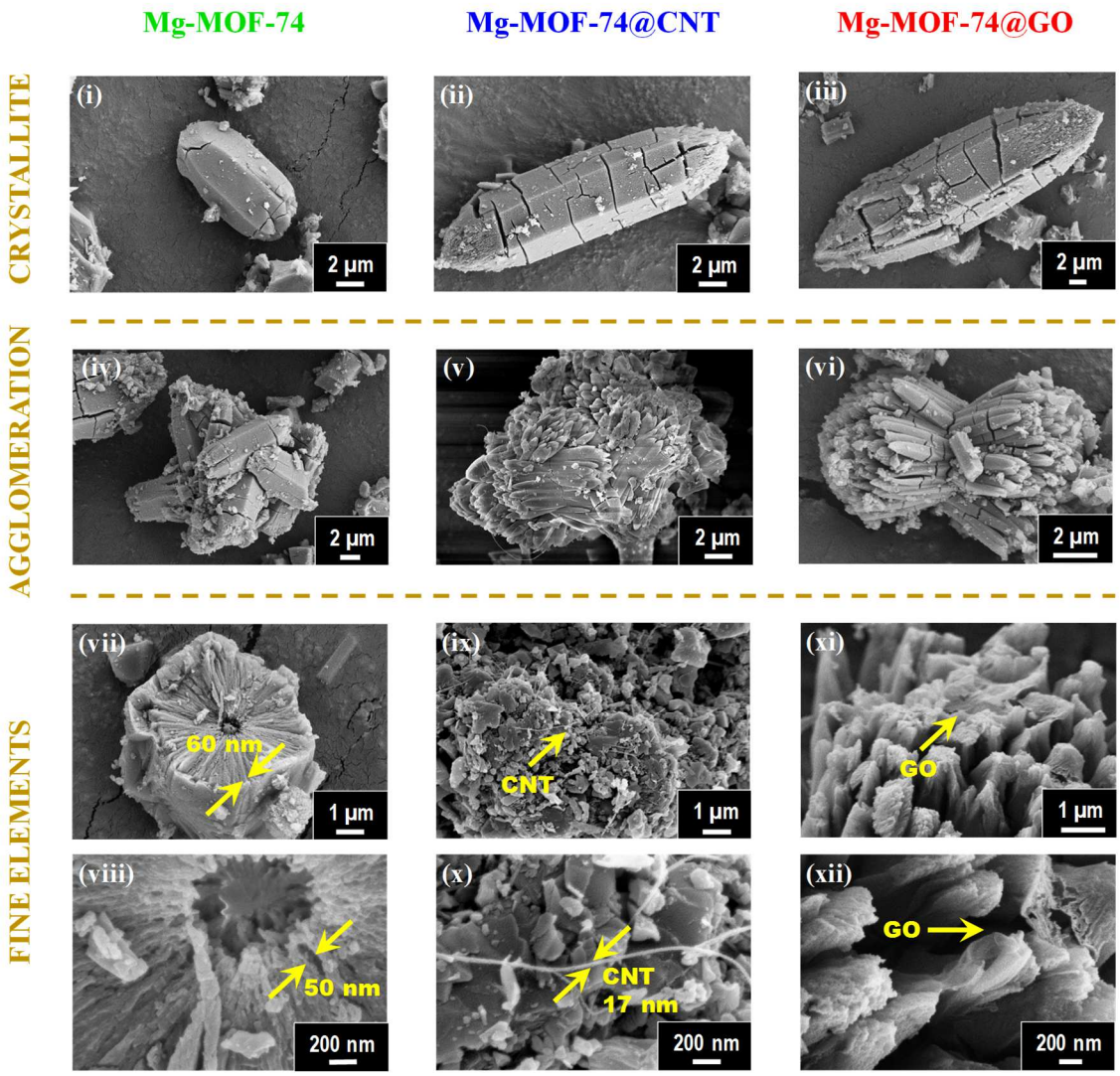

Figure 3. Micrograph images of Mg-MOF-74, Mg-MOF- 74@CNT and Mg-MOF-74@GO.

TGA analysis was performed in order to evaluate the thermal stability of the synthesized materials. Figure 4 illustrates TGA plots of all synthesized materials which agree well with the profile of the same material in other literature [48] showing two notable weight loss steps: (i) 50-250°C due to the removal of moisture and guest molecules present in the micropores and (ii) above 450 °C attributed to the decomposition of organic fragments in the material.

Several works have shown a plateau between 200 and 400 °C for freshly-prepared well-activated MOF-74 systems [13, 43, 49, 50]. However, numerous studies report less steep weight loss profiles, probably due to the presence of the residual reactants enclosed in materials' micropores or their partial oxidation [41, 51-54]. Comparing TGA curves in Figure 4, one can realize faster weight loss upon heating (between 200 and 400 °C) for pristine MOF-74 in comparison to its composites, which can indicate more pronounced pore blocking of the former with reactants, due to incomplete activation. High thermal stability of Mg-MOF-74 was earlier claimed by Britt et al. (2009) stating that it could sustain high temperatures up to 400°C [16]. Regarding the high-temperature domain where the material rupture occurs, it can be realized that the pristine material having more steep trend degrades more rapidly in comparison to carbon-doped composites. The slight nanostructure modification or defects in Mg-MOF-74@CNT and Mg-MOF-74@GO as revealed in the qualitative and morphological analysis gives advantage on the thermal stability behavior of the composites in comparison to the pristine material. In the case of the pristine material, drastic weight losses above 550°C appear also are in line with the assumption that residual free ligand should have remained within the porous structure.

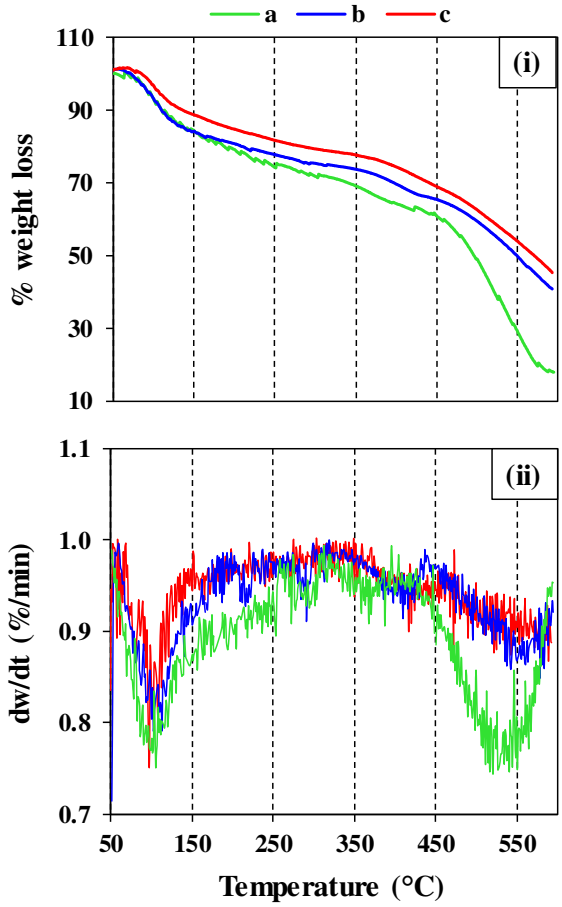

Figure 4. (i) TGA plots and (ii) their derivatives of (a) Mg-MOF-74, (b) Mg-MOF-74@CNT and (c) Mg-MOF-74@GO.

N_2 physisorption analysis at 77 K was carried out to assess specific surface areas and pore volumes of the materials. Figure 5i presents N_2 adsorption/desorption isotherms of all synthesized materials acquired at $10^{-7} \leq p/p^{\circ} \leq 1$. The measured data features Type I-Type IV isotherm with a pseudo-plateau at $10^{-7} \leq p/p^{\circ} \leq 0.1$ suggesting the completion of micropore filling, and marginal hysteresis loop between adsorption and desorption isotherms at $0.4 \leq p/p^{\circ} \leq 1$ due to the occurrence of capillary condensation which is the characteristic of mesopores. Despite being criticized for its well-known shortcomings, the BET (Brunauer, Emmett, and Teller) model is considered as a standard and continuously being used to assess

specific surface areas of microporous materials. The model is reliable provided that three consistency criteria are verified : (i) the BET constant must be positive indicating the valid range of the BET equation, (ii) application of the fitting must be limited to the range where $V(1-p/p^o)$ continuously increases with p/p^o, and, (iii) the BET monolayer capacity must fall within the pressure region selected for the calculation [55]. Walton and Snurr [56] revisited the applicability of the BET model to MOF materials using grand canonical Monte Carlo simulations. These authors conclude that despite these MOFs possess surfaces that are far from flat, the BET model is valid over the pressure range identified by established consistency criteria. For MOF materials, that relative pressure range may include data corresponding to the first steps of the adsorption isotherm less than 0.01, so falling far below the "standard" BET pressure range of [0.05 – 0.3]. Therefore, BET model affords the apparent values of 1370 m^2/g, 1660 m^2/g and 1720 m^2/g for Mg-MOF-74, Mg-MOF-74@CNT and Mg-MOF-74@GO, respectively. Details for the determination of the specific surface areas of the materials measured after 12 months of ageing are given in the Supporting Information (Figure S2-1). The specific surface area of Mg-MOF-74 pristine material is not as high as reported elsewhere, 1775 m^2/g in [42]. This discrepancy may be attributed to the lower activation temperature applied in our synthesis protocol, 150 °C instead of 250 °C, leading to incomplete solvent washing as previously suggested in the analysis of the IR spectrum showing a slight shoulder merging at the1590 cm^{-1} peak. Despite sealed inert storage conditions in sealed bags under vacuum, it is not excluded that very few air leakages may have occurred and generated some partial oxidation of the aged pristine samples. However, both XRD and BET analysis did not confirm that assumption. It is noted a good accordance with experimental 77K-N_2 adsorption isotherm data reported by Glover et al. [57] but some disagreement with the data

collected by Bao et al. [13]. As low pressure range was excluded from the BET analysis carried out by these authors, reported specific surface area were underestimated and computed around 1200 m^2/g.

Characterization of micropore size and volume distribution using gas adsorption relies exclusively on isotherm modelling accounting for solid surface–gas molecule interaction, gas molecule–gas molecule interaction and confinement of pore size [58]. Since MOFs feature a large range of electronic properties and energies of adsorption sites, to date, the accurate determination of their micropore sizes from gas adsorption isotherms is difficult due to the lack of adequate models. Several published works have proposed to use conventional models like Density Functional Theory [59] or Horvath-Kawazoe [13] optimized for zeolites to assess micropore size in MOFs (see Supporting Information for more details). In the present work we will mainly rely on the raw data of N_2 adsorption for describing micropore filling processes. High-resolution N_2 adsorption isotherms and their derivatives, offering better sensitivity to adsorbed amount variation with the pressure, are shown in Figure 5ii. At least three well-defined components in micropore filling domain can be distinguished: (i) a narrow contribution with the maximum at $p/p°=5\cdot10^{-7}$-$8\cdot10^{-7}$ and two broad contributions with the maxima at (ii) $p/p°=5\cdot10^{-5}$-$8\cdot10^{-5}$ and (iii) $p/p°=10^{-3}$. According to the crystallographic structure, Mg-MOF-74 features a unique size of micropore close to 10 Å [14]. Comparing the literature data for MOF-74 and other well-crystallized MOF materials with pore size close to 10 Å [60], their micropore filling with N_2 at 77 K is usually completed before $p/p°=10^{-4}$-10^{-3}, so the first two contributions laying in “low-pressure” domain are assigned to structural microporosity. The origin of the splitting of micropore filling processes into two components with nearly close population could be due to the coexistence of two adsorption sites with

different binding energy values (as determined for H_2, CO_2 and other gases by molecular modeling) referred as “near-metal” and “near-ligand” featuring one-to-one ratio [11, 14, 17]. The increase of the amount of adsorbed nitrogen below $p/p°=10^{-3}$ for both composites, in comparison to the pristine material, is in line with better accessibility of microporous volume of the former. For both Mg-MOF-74 composites, the N_2 adsorption isotherms are shifted to lower relative pressures suggesting higher adsorbates–adsorbent interaction energies. Meanwhile, the “high-pressure” contributions with the maximum at $p/p°=10^{-3}$ are assigned to larger intercrystallite pores, the volume of which slightly increases upon doping with carbonaceous agents. This tendency is in line with the finding of different works reported that carbonaceous agents such as GO and CNT act as binders favoring the formation of new micropores [12, 21-33].

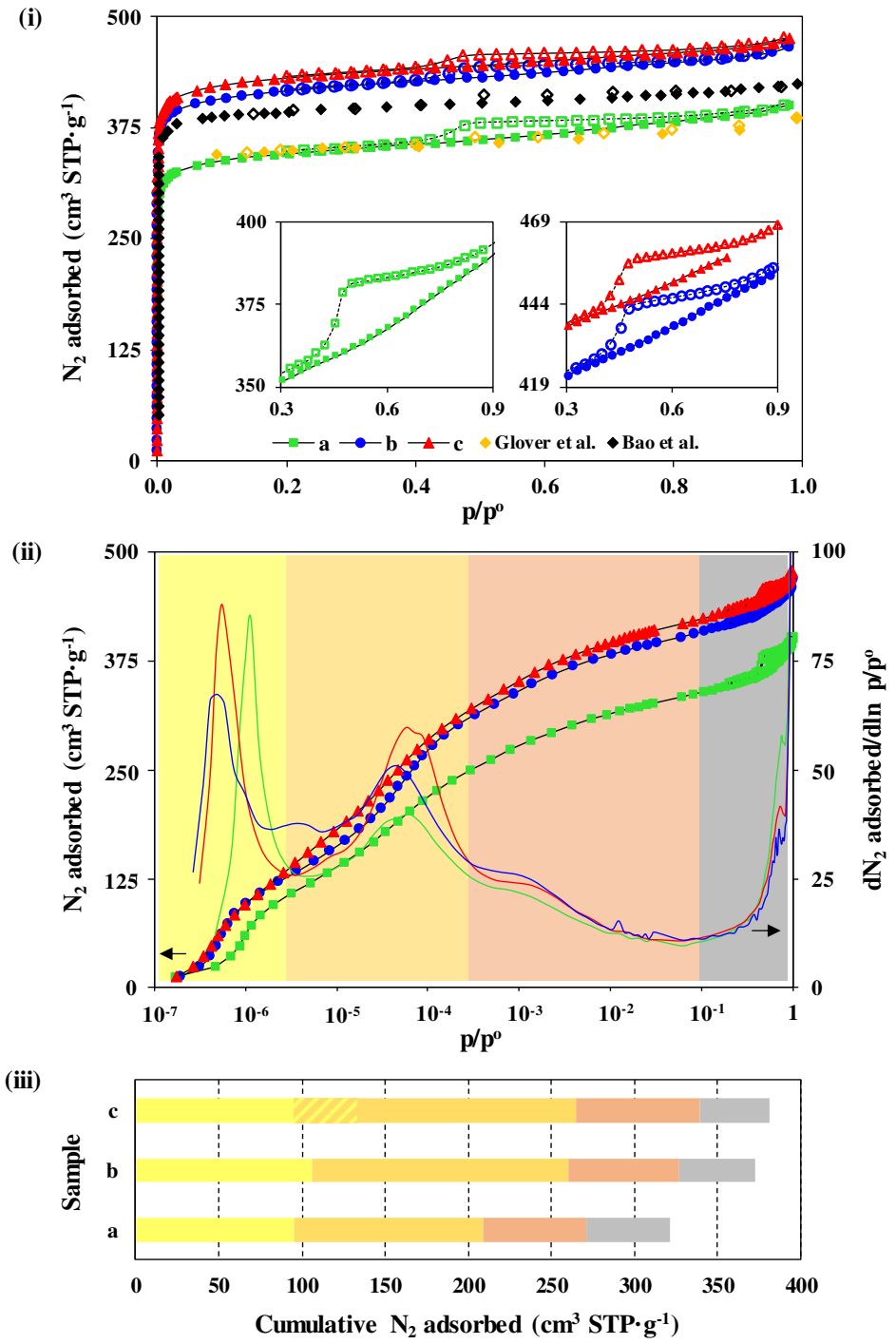

Figure 5. (i) N_2 ads/desorption isotherms at 77 K, (ii) their derivatives and (iii) cumulative N_2 adsorbed volume of (a) Mg-MOF-74, (b) Mg-MOF-74@CNT and (c) Mg-MOF-74@GO. Solid and open symbols represent the adsorption and desorption of N_2, respectively.

In order to complete the material characterization, equilibrium data of CO_2 adsorption were measured at 1 bar and 25 °C. The isotherms presented in Figure 6 reveal the larger CO_2 uptake obtained with Mg-MOF-74@CNT and Mg-MOF-74@GO, increased by 18 mol% and 23 mol% respectively compared with the pristine Mg-MOF-74. This result is in accordance with the enhancement of the pore textural properties in both carbon composites.

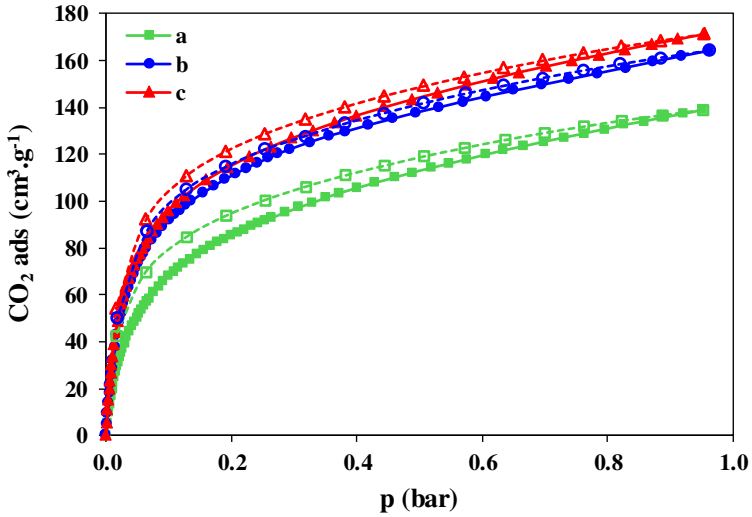

Figure 6. CO_2 ads/desorption isotherms at 1 bar and 25 °C of (a) Mg-MOF-74, (b) Mg-MOF-74@CNT and (c) Mg-MOF-74@GO fitted to dual-site Langmuir model. Solid and open symbols represent the adsorption and desorption, respectively.

Conclusion:

Mg-MOF-74 and its carbon-based composites, Mg-MOF-74@CNT and Mg-MOF-74@GO, were successfully synthesized using solvothermal method with 0.3 wt% of substitution of carbonaceous agent. The crystallinity of Mg-MOF-74 was well preserved in both composites but Mg-MOF-74@CNT and Mg-MOF-74@GO appeared with larger average crystallite sizes, 82 nm and 73 nm respectively compared to 67 nm for the pristine material. A slight defect in crystal nanostructure could be proposed knowing that both composites exhibited reduced intensity of principal peaks in XRD signals. The morphology showed that Mg-MOF-74@CNT and Mg-MOF-74@GO displayed larger average particle sizes of single specimen, 23 µm and 37 µm respectively compared to 10 µm for the pristine material. CNT and GO promoted agglomeration of polycrystalline structure of Mg-MOF-74 during the crystal growth by interlocking with the framework and stacking to the crystallites surface. The structure modification in the Mg-MOF-74 composites not only gave advantage on thermal stability but also popularized new formation of micropores inside MOFs. The BET specific surface area was increased from 1111 m^2/g measured for the pristine Mg-MOF-74 to 1340 m^2/g (increased by 20.6%) and 1393 m^2/g (by 25.4%) for Mg-MOF-74@CNT and Mg-MOF-74@GO, respectively. Calculated using DFT, the results were coherent with the increased micropore volumes from 0.40 cm^3/g for the pristine Mg-MOF-74 to 0.48 cm^3/g (by 18.0%) and 0.49 cm^3/g (by 23.9%) for Mg-MOF-74@CNT and Mg-MOF-74@GO, respectively. The uptake of CO_2 adsorption at 1 bar and 25 °C was improved by 18 mol% and 23 mol% for Mg-MOF-74@CNT and Mg-MOF-74@GO, respectively, compared with the pristine Mg-MOF-74. This current work proved that by doping with carbonaceous agents, particle morphology and pore textural properties of Mg-MOF-74 were substantially

modified inducing larger gas adsorption capacities.

Acknowledgment:

The authors thank the Carbon Dioxide Research Center, Department of Chemical Engineering, Universiti Teknologi PETRONAS and the Department of Energy Systems and Environment (GEPEA laboratory), IMT Atlantique, for their support in this collaborative work. The funds granted by University Research Internal Funding (Grant No. URIF 0153 AA-B90), Yayasan UTP (Grant No. YUTP 0153AA-H42), Prototype Research Grant Scheme (Grant No. PRGS/1/2017/TK02/UTP/02/1) and IMT Atlantique (half-PhD scholarship).

References:

[1] Y. Yusran, D. Xu, Q. Fang, D. Zhang, and S. Qiu, "MOF-derived Co@NC nanocatalyst for catalytic reduction of 4-nitrophenol to 4-aminophenol," *Microporous and Mesoporous Materials,* vol. 241, pp. 346-354, 2017.

[2] P. Horcajada, C. Serre, M. Vallet‐Regí, M. Sebban, F. Taulelle, and G. Férey, "Metal-organic frameworks as efficient materials for drug delivery," *Angewandte Chemie International Edition,* vol. 118, no. 36, pp. 6120-6124, 2006.

[3] N. A. Khan, Z. Hasan, and S. H. Jhung, "Adsorptive removal of hazardous materials using metal-organic frameworks (MOFs): A review," *Journal of Hazardous Materials,* vol. 244, pp. 444-456, 2013.

[4] E. Ahmed, A. Deep, E. E. Kwon, R. J. C. Brown, and K.-H. Kim, "Performance comparison of MOF and other sorbent materials in removing key odorants emitted from pigpen slurry," *Scientific Reports,* vol. 6, pp. 1-11, 2016.

[5] B. Liu, H. Shioyama, H. Jiang, X. Zhang, and Q. Xu, "Metal-organic framework (MOF) as a template for syntheses of nanoporous carbons as electrode materials for supercapacitor," *Carbon,* vol. 48, no. 2, pp. 456-463, 2010.

[6] H. Furukawa, N. Ko, Y. B. Go, N. Aratani, S. B. Choi, E. Choi, A. Ö. Yazaydin, R. Q. Snurr, M. O'Keeffe, and J. Kim, "Ultrahigh porosity in metal-organic frameworks," *Science,* vol. 329, no. 5990, pp. 424-428, 2010.

[7] C. Dey, T. Kundu, B. P. Biswal, A. Mallick, and R. Banerjee, "Crystalline metal-organic frameworks (MOFs): Synthesis, structure and function," *Acta Crystallographica Section B: Structural Science, Crystal Engineering And Materials,* vol. 70, no. 1, pp. 3-10, 2014.

[8] J. L. Rowsell, and O. M. Yaghi, "Metal-organic frameworks: A new class of porous materials," *Microporous and Mesoporous Materials,* vol. 73, no. 1, pp. 3-14, 2004.

[9] M. Hu, "Design, synthesis and applications of metal organic frameworks," Worcester Polytechnic Institute, 2011.

[10] S. Chaemchuen, N. A. Kabir, K. Zhou, and F. Verpoort, "Metal–organic frameworks for upgrading biogas via CO_2 adsorption to biogas green energy," *Chemical Society Reviews,* vol. 42, no. 24, pp. 9304-9332, 2013.

[11] L. Valenzano, B. Civalleri, S. Chavan, G. T. Palomino, C. O. Areán, and S. Bordiga, "Computational and experimental studies on the adsorption of CO, N_2, and CO_2 on Mg-MOF-74," *The Journal of Physical Chemistry C,* vol. 114, no. 25, pp. 11185-

11191, 2010.
[12] D.-L. Chen, H. Shang, W. Zhu, and R. Krishna, "Transient breakthroughs of CO_2/CH_4 and C_3H_6/C_3H_8 mixtures in fixed beds packed with Ni-MOF-74"," *Chemical Engineering Science*, vol. 117, pp. 407-415, 2014.
[13] Z. Bao, L. Yu, Q. Ren, X. Lu, and S. Deng, "Adsorption of CO_2 and CH_4 on a magnesium-based metal organic framework," *Journal of Colloid and Interface Science,* vol. 353, no. 2, pp. 549-556, 2011.
[14] D.-A. Yang, H.-Y. Cho, J. Kim, S.-T. Yang, and W.-S. Ahn, "CO_2 capture and conversion using Mg-MOF-74 prepared by a sonochemical method," *Energy & Environmental Science,* vol. 5, no. 4, pp. 6465-6473, 2012.
[15] D. Banerjee, H. Wang, B. J. Deibert, and J. Li, "Chapter 4: Alkaline earth metal-based metal-organic frameworks: Synthesis, Properties and Applications," *The chemistry of metal-organic frameworks: Synthesis, characterization, and applications*, S. Kaskel, ed., pp. 73-99, Hoboken, New Jersey, United States: John Wiley & Sons, 2016.
[16] D. Britt, H. Furukawa, B. Wang, T. G. Glover, and O. M. Yaghi, "Highly efficient separation of carbon dioxide by a metal-organic framework replete with open metal sites," *Proceedings of the National Academy of Sciences,* vol. 106, no. 49, pp. 20637-20640, 2009.
[17] M. Lopez, P. Canepa, and T. Thonhauser, "NMR study of small molecule adsorption in MOF-74-Mg," *The Journal of Chemical Physics,* vol. 138, no. 15, pp. 154704, 2013.
[18] I. Ahmed, and S. H. Jhung, "Composites of metal-organic frameworks: Preparation and application in adsorption," *Materials Today,* vol. 17, no. 3, pp. 136-146, 2014.
[19] X.-W. Liu, T.-J. Sun, J.-L. Hu, and S.-D. Wang, "Composites of metal-organic frameworks and carbon-based materials: Preparations, functionalities and applications," *Journal of Materials Chemistry A,* vol. 4, no. 10, pp. 3584-3616, 2016.
[20] Y. Liu, Z. U. Wang, and H. C. Zhou, "Recent advances in carbon dioxide capture with metal‐organic frameworks," *Greenhouse Gases: Science and Technology,* vol. 2, no. 4, pp. 239-259, 2012.
[21] C. Petit, B. Levasseur, B. Mendoza, and T. J. Bandosz, "Reactive adsorption of acidic gases on MOF/graphite oxide composites," *Microporous and Mesoporous Materials,* vol. 154, pp. 107-112, 2012.
[22] Y. Zhao, Y. Cao, and Q. Zhong, "CO_2 capture on metal-organic framework and graphene oxide composite using a high-pressure static adsorption apparatus," *Journal Of Clean Energy Technologies,* vol. 2, no. 1, pp. 34-37, 2014.
[23] C. Petit, B. Mendoza, and T. J. Bandosz, "Reactive adsorption of ammonia on Cu-based MOF/graphene composites," *Langmuir,* vol. 26, no. 19, pp. 15302-15309, 2010.
[24] C. Petit, B. Mendoza, and T. J. Bandosz, "Hydrogen sulfide adsorption on MOFs and MOF/graphite oxide composites," *ChemPhysChem,* vol. 11, no. 17, pp. 3678-3684, 2010.
[25] S. J. Yang, J. H. Cho, K. S. Nahm, and C. R. Park, "Enhanced hydrogen storage capacity of Pt-loaded CNT@MOF-5 hybrid composites," *International Journal Of Hydrogen Energy,* vol. 35, no. 23, pp. 13062-13067, 2010.
[26] S. J. Yang, J. Y. Choi, H. K. Chae, J. H. Cho, K. S. Nahm, and C. R. Park, "Preparation and enhanced hydrostability and hydrogen storage capacity of CNT@MOF-5 hybrid composite," *Chemistry of Materials,* vol. 21, no. 9, pp. 1893-1897, 2009.
[27] M. Anbia, and V. Hoseini, "Development of MWCNT@MIL-101 hybrid composite with enhanced adsorption capacity for carbon dioxide," *Chemical Engineering Journal,* vol. 191, pp. 326-330, 2012.
[28] A. K. Adhikari, and K.-S. Lin, "Improving CO_2 adsorption capacities and CO_2/N_2 separation efficiencies of MOF-74 (Ni, Co) by doping palladium-containing activated carbon," *Chemical Engineering Journal,* vol. 284, pp. 1348-1360, 2016.
[29] V. Jabbari, J. Veleta, M. Zarei-Chaleshtori, J. Gardea-Torresdey, and D. Villagrán, "Green synthesis of magnetic MOF@GO and MOF@CNT hybrid nanocomposites with high adsorption capacity towards organic pollutants," *Chemical Engineering Journal,* vol. 304, pp. 774-783, 2016.
[30] H. Askari, M. Ghaedi, K. Dashtian, and M. H. A. Azghandi, "Rapid and high-capacity ultrasonic assisted adsorption of ternary toxic anionic dyes onto MOF-5-activated carbon: Artificial neural networks, partial least squares, desirability function and isotherm and kinetic study," *Ultrasonics Sonochemistry,* vol. 37, pp. 71-82, 2017.
[31] R.-H. Shi, Z.-R. Zhang, H.-L. Fan, T. Zhen, J. Shangguan, and J. Mi, "Cu-based metal-organic framework/activated carbon composites for sulfur compounds removal," *Applied Surface Science,* vol. 394, pp. 394-402, 2017.
[32] Z. Yu, J. Deschamps, L. Hamon, P. K. Prabhakaran, and P. Pré, "Hydrogen adsorption and kinetics in MIL-101 (Cr) and hybrid activated carbon-MIL-101 (Cr) materials," *International Journal of Hydrogen Energy,* vol. 42, no. 12, pp. 8021-8031, 2017.
[33] W. Huang, X. Zhou, Q. Xia, J. Peng, H. Wang, and Z. Li, "Preparation and adsorption performance of GrO@Cu-BTC for separation of CO_2/CH_4," *Industrial & Engineering Chemistry Research,* vol. 53, no. 27, pp. 11176-11184, 2014.
[34] S. Ullah, M. A. Bustam, A. G. Al-Sehemi, M. A. Assiri, F. A. A. Kareem, A. Mukhtar, M. Ayoub, and G. Gonfa, "Influence of post-synthetic graphene oxide (GO) functionalization on the selective CO_2/CH_4 adsorption behavior of MOF-200 at different temperatures; an experimental and adsorption isotherms study," *Microporous Mesoporous Materials*, pp. 110002, 2020.
[35] A. Corma, and H. Garcia, "Supramolecular host‐guest systems in zeolites prepared by ship‐in‐a‐bottle synthesis,"

European Journal of Inorganic Chemistry, vol. 2004, no. 6, pp. 1143-1164, 2004.

[36] M. H. Alkordi, Y. Liu, R. W. Larsen, J. F. Eubank, and M. Eddaoudi, "Zeolite-like metal-organic frameworks as platforms for applications: On metalloporphyrin-based catalysts," *Journal of the American Chemical Society,* vol. 130, no. 38, pp. 12639-12641, 2008.

[37] K. Kamal, M. A. Bustam, M. Ismail, D. Grekov, A. Mohd Shariff, and P. Pré, "Optimization of Washing Processes in Solvothermal Synthesis of Nickel-Based MOF-74," *Materials,* vol. 13, no. 12, pp. 2741, 2020.

[38] H. Furukawa, K. E. Cordova, M. O'Keeffe, and O. M. Yaghi, "The chemistry and applications of metal-organic frameworks," *Science,* vol. 341, no. 6149, pp. 1230444, 2013.

[39] S. A. Speakman, "Profile Fitting for Analysis of XRPD Data using HighScore Plus v3," *Massachusetts Institute of Technology, Cambridge MA*, 2012.

[40] P. D. Dietzel, R. Blom, and H. Fjellvåg, "Base‐induced formation of two magnesium metal‐organic framework compounds with a bifunctional tetratopic ligand," *European Journal of Inorganic Chemistry,* vol. 2008, no. 23, pp. 3624-3632, 2008.

[41] P. D. Dietzel, R. E. Johnsen, R. Blom, and H. Fjellvåg, "Structural changes and coordinatively unsaturated metal atoms on dehydration of honeycomb analogous microporous metal-organic frameworks," *Chemistry–A European Journal,* vol. 14, no. 8, pp. 2389-2397, 2008.

[42] J. B. DeCoste, G. W. Peterson, B. J. Schindler, K. L. Killops, M. A. Browe, and J. J. Mahle, "The effect of water adsorption on the structure of the carboxylate containing metal–organic frameworks Cu-BTC, Mg-MOF-74, and UiO-66," *Journal of Materials Chemistry A,* vol. 1, no. 38, pp. 11922-11932, 2013.

[43] S. A. FitzGerald, B. Burkholder, M. Friedman, J. B. Hopkins, C. J. Pierce, J. M. Schloss, B. Thompson, and J. L. C. Rowsell, "Metal-Specific Interactions of H2 Adsorbed within Isostructural Metal–Organic Frameworks", *Journal of the American Chemical Society,* vol. 133, no. 50, pp. 20310–20318, 2011.

[44] K. Tan, S. Zuluaga, Q. Gong, P. Canepa, H. Wang, J. Li, Y. J. Chabal and T. Thonhauser, "Water Reaction Mechanism in Metal Organic Frameworks with Coordinatively Unsaturated Metal Ions: MOF-74", *Chem. Mater.*, vol. 26, no. 23, pp. 6886–6895, 2014.

[45] B. H. Stuart, "Chapter 2: Organic molecules," *Infrared spectroscopy: Fundamentals and applications*, pp. 71-93, Hoboken, New Jersey, United States: John Wiley & Sons, 2004.

[46] N. Maksimchuk, M. Timofeeva, M. Melgunov, A. Shmakov, Y. A. Chesalov, D. Dybtsev, V. Fedin, and O. Kholdeeva, "Heterogeneous selective oxidation catalysts based on coordination polymer MIL-101 and transition metal-substituted polyoxometalates," *Journal of Catalysis,* vol. 257, no. 2, pp. 315-323, 2008.

[47] C. Petit, J. Burress, and T. J. Bandosz, "The synthesis and characterization of copper-based metal-organic framework/graphite oxide composites," *Carbon,* vol. 49, no. 2, pp. 563-572, 2011.

[48] S. R. Caskey, A. G. Wong-Foy, and A. J. Matzger, "Dramatic tuning of carbon dioxide uptake via metal substitution in a coordination polymer with cylindrical pores," *Journal of the American Chemical Society,* vol. 130, no. 33, pp. 10870-10871, 2008.

[49] M. Díaz-García, M. Sánchez-Sánchez, Synthesis and characterization of a new Cd-based metal-organicframework isostructural with MOF-74/CPO-27 materials, *Microporous and Mesoporous Materials*, vol. 190, pp. 248-254, 2014.

[50] M. H. Rosnes, B. Pato-Doldán, R. E. Johnsen, A. Mundstock, J. Caro, P. D. C. Dietzel, Role of the metal cation in the dehydration of the microporous metal–organic frameworks CPO-27-M, *Microporous and Mesoporous Materials*, vol. 309, 110503, 2020.

[51] S. Pu, J. Wang, L. Li, Z. Zhang, Z. Bao, Q. Yang, Y. Yang, H. Xing, and Q. Ren, Performance Comparison of Metal–Organic Framework Extrudates and Commercial Zeolite for Ethylene/Ethane Separation, *Ind. Eng. Chem. Res.*, vol. 57, no. 5, pp. 1645–1654, 2018.

[52] D. Villarroel-Rocha, A. A. Godoy, C. Toncon-Leal, J. Villarroel-Rocha, M. S. Moreno, M. C. Bernini, G. E. Narda, and K. Sapag, Synthesis of micro–mesoporous CPO-27-Mg@KIT-6 composites and their test in CO2 adsorption, *New J. Chem.*, vol. 44, pp. 10056-10065, 2020.

[53] M. C. Bernini, A. A. García Blanco, J. Villarroel-Rocha, D. Fairen-Jimenez, K. Sapag, A. J. Ramirez-Pastor, and G. E. Narda, Tuning the target composition of amine-grafted CPO-27-Mg for capture of CO2 under post-combustion and air filtering conditions: a combined experimental and computational study, *Dalton Trans.*, vol. 44, pp. 18970-18982, 2015.

[54] H.-S. Moon, J.-H. Moon, D. Hyuk Chun, Y. Cheol Park, Y. No Yun, M. Sohail, K. Baek, H. Kim, Synthesis of [Mg2(DOBDC)(DMF)2]@polystyrene composite and its carbon dioxide adsorption, *Microporous and Mesoporous Materials*, vol. 232, pp. 161-166, 2016.

[55] J. Rouquerol, P. Llewellyn, and F. Rouquerol, "Is the BET equation applicable to microporous adsorbents," *Stud. Surf. Sci. Catal,* vol. 160, no. 07, pp. 49-56, 2007.

[56] K. S. Walton, and R. Q. Snurr, “Applicability of the BET method for determining surface areas of microporous metal– organic frameworks,” *Journal of the American Chemical Society,* vol. 129, no. 27, pp. 8552-8556, 2007.

[57] T. G. Glover, G. W. Peterson, B. J. Schindler, D. Britt, and O. Yaghi, “MOF-74 building unit has a direct impact on toxic gas adsorption,” *Chemical Engineering Science,* vol. 66, no. 2, pp. 163-170, 2011.

[58] M. Thommes, and K. A. Cychosz, “Physical adsorption characterization of nanoporous materials: Progress and challenges,” *Adsorption,* vol. 20, no. 2-3, pp. 233-250, 2014.

[59] X. Sun, Q. Xia, Z. Zhao, Y. Li, and Z. Li, “Synthesis and adsorption performance of MIL-101(Cr)/graphite oxide composites with high capacities of n-hexane,” *Chemical Engineering Journal,* vol. 239, pp. 226-232, 2014.

[60] I. Senkovska, K. A. Cychosz, P. Llewellyn, M. Thommes, and S. Kaskel, "Chapter 19: Adsorption Methodology," *The chemistry of metal-organic frameworks: Synthesis, characterization, and applications*, S. Kaskel, ed., pp. 575-605: John Wiley & Sons, 2016.

Graphical Abstract: